

Nature of the antiferromagnetic and nematic transitions in $\text{Sr}_{1-x}\text{Ba}_x\text{Fe}_{1.97}\text{Ni}_{0.03}\text{As}_2$

Dongliang Gong,^{1,2} Zhaoyu Liu,^{1,2} Yanhong Gu,^{1,2} Tao Xie,^{1,2}
Xiaoyan Ma,^{1,2} Huiqian Luo,¹ Yi-feng Yang,^{1,2,3} and Shiliang Li^{1,2,3,*}

¹*Beijing National Laboratory for Condensed Matter Physics,
Institute of Physics, Chinese Academy of Sciences, Beijing 100190, China*

²*School of Physical Sciences, University of Chinese Academy of Sciences, Beijing 100190, China*

³*Collaborative Innovation Center of Quantum Matter, Beijing 100190, China*

We have systematically studied the antiferromagnetic and nematic transitions in $\text{Sr}_{1-x}\text{Ba}_x\text{Fe}_{1.97}\text{Ni}_{0.03}\text{As}_2$ by magnetic susceptibility and uniaxial-pressure resistivity measurements, respectively. The derivatives of the temperature dependence of both magnetic and nematic susceptibilities show clearly sharp peaks when the transitions are first order. Accordingly, we show that while both of the magnetic and nematic transitions change from first order to second order with increasing Barium doping level, there is a narrow doping range where the former becomes second order but the latter remains first order, which has never been realized before in other systems. Moreover, the antiferromagnetic and nematic transition temperatures become different and the jump of nematic susceptibility becomes small in this intermediate doping range. Our results provide key information on the interplay between magnetic and nematic transitions. Concerning the current debate on the microscopic models for nematicity in iron-based superconductors, these observations agree with the magnetic scenario for an itinerant fermionic model.

PACS numbers:

I. INTRODUCTION

The nature of the antiferromagnetic (AF) and nematic transitions in iron-based superconductors has attracted much interest. The underlying mechanism of both orders may be crucial to our understanding of superconductivity in these materials¹. The establishment of the electronic nematic order, which breaks the four-fold rotational symmetry of the underlying lattice, is always accompanied by a structural phase transition due to the symmetry constraint. Theoretical understanding of these phase transitions can be mainly divided into two groups based on the spin or orbital degree of freedom depending on the microscopic driving force of the nematic order. In the orbital scenario, the orbital ordering gives rise to the structural transition and then triggers the magnetic transition at the same or lower temperature²⁻⁵. In the spin scenario, on the other hand, it has been argued that magnetic fluctuations are of primary responsibility for triggering the nematic instability, although it is still not clear whether a correct microscopic theory should be built solely on a local spin model or the itinerant characteristic of the Fe $3d$ electrons should be taken into full account⁶⁻¹⁴.

One way to test these theories is to carefully compare their predictions with experimental results. Especially, the nature of these transitions can reveal crucial information on the origin of the nematic order. The rich phase diagrams of the electron-doped “122” systems, i.e., AFe_2As_2 ($A = \text{Ca}, \text{Sr}, \text{Ba}$) and its electron doped materials, give us an opportunity to do so. Both the magnetic and structural transitions in CaFe_2As_2 and SrFe_2As_2 are strongly first order and happen at the same temperature¹⁵⁻¹⁷. For BaFe_2As_2 , while the nature of these two transitions were initially under debate¹⁸⁻²¹, further detailed studies have suggested that the struc-

tural transition is second order followed by a first order magnetic transition^{6,22}. Doping electron carriers (Co or Ni) into BaFe_2As_2 makes both transitions second order²³⁻²⁷. Therefore, a magnetic tricritical point has been suggested where the AF transition changes from first to second order with the structural transition remaining second order^{6,28}, but a nematic tricritical point has not been reported. Moreover, an intermediate phase where a first order nematic transition followed by a second order AF transition has never been found.

In this paper, we give detailed studies on the phase diagram of $\text{Sr}_{1-x}\text{Ba}_x\text{Ni}_{0.03}\text{Fe}_{1.97}\text{As}_2$ by measuring the resistivity, magnetic susceptibility and nematic susceptibility. It has been shown that Ba doping into SrFe_2As_2 can continuously reduce both the magnetic and structural transition temperatures²⁹. We doped 1.5% of Ni into the system, where the AF and nematic transitions in the $x = 0$ sample are still first order but those in the $x = 1$ sample are clearly second order³⁰. The crossover from first order to second order transition happens at different doping levels for magnetic and nematic systems. In this intermediate region, although the nematic transition is first order, the jump of the nematic susceptibility becomes significantly small. These observations are consistent with the theory based on the magnetic scenario for an itinerant fermionic model in excellent details¹¹.

II. EXPERIMENTS

Single crystals of $\text{Sr}_{1-x}\text{Ba}_x\text{Ni}_{0.03}\text{Fe}_{1.97}\text{As}_2$ samples were grown by the self-flux methods as reported previously³¹. The magnetic susceptibility measurements were carried out on the magnetic property measurement system (MPMS) at 7 Tesla applied within the a-

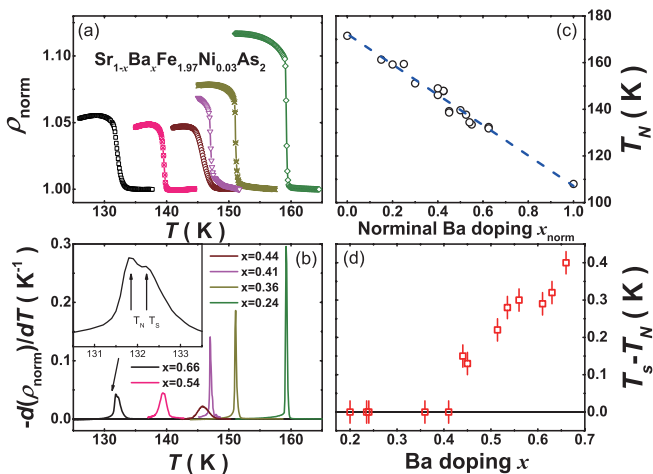


FIG. 1: (a) Normalized in-plane resistivity ρ_{norm} of $\text{Sr}_{1-x}\text{Ba}_x\text{Ni}_{0.03}\text{Fe}_{1.97}\text{As}_2$. The values are normalized to those at about 5 K higher than T_N for convenience. (b) Temperature dependence of $-d(\rho_{\text{norm}})/dT$ showing sharp and broad peaks around T_N at low and high doping levels, respectively. In sufficiently high doping samples such as $x = 0.66$, the splitting between the magnetic and structural transitions results in two peaks as shown in the inset. (c) Relationship between T_N and nominal doping x_{norm} . The dashed line is a linear fit to the data. (d) Doping dependence of $T_s - T_N$. The error bars are manually set to 0.03 K, which is much larger than fitted error bars from the two Lorentz fitting as described in the main text.

b plane. Both the resistivity and nematic susceptibility were measured on the physical property measurement system (PPMS). The samples were cut into thin rectangular plates along the tetragonal (1,1,0) direction. After measuring the resistivity at zero pressure, the samples were glued on a home-made uniaxial pressure device as reported elsewhere³². The pressure is estimated from previous measurements³². In all measurements, the temperature was stabilized long enough to obtain reliable data.

III. RESULTS AND DISCUSSIONS

Figure 1(a) gives the temperature dependence of the in-plane resistivity ρ_{norm} normalized by its value at about 5 K above the AF transition temperature T_N . A jump around T_N for lower doping samples can be easily seen, suggesting the first order nature of the transitions. As shown previously^{23,31}, the precise values of T_N and the structural transition temperature T_s can be determined from the first derivative of ρ_{norm} [Fig. 1(b)]. For lower doping samples where both transitions are first order and happen at the same temperature, a very sharp peak appears. When the magnetic and structural transitions are well separated, two peaks can be observed corresponding to T_N and T_s as shown in the inset of Fig. 1(b). In the intermediate region where the separation is not obvious,

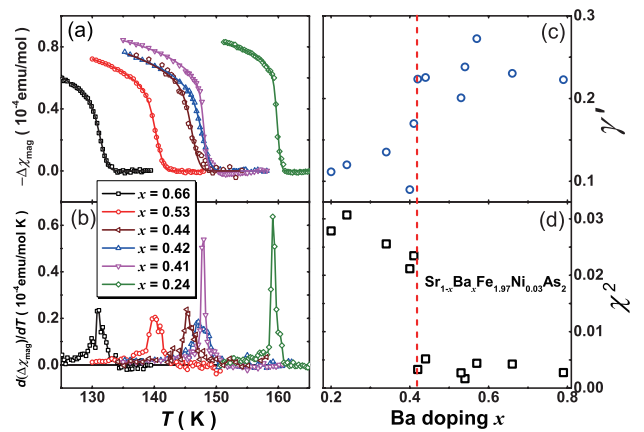


FIG. 2: (a) Temperature dependence of subtracted magnetic susceptibility $-\Delta\chi_{\text{mag}}$. Here $\Delta\chi_{\text{mag}} = \chi_{\text{mag}} - \chi_{bg}$, where χ_{bg} is the linear background. The solid lines are fitted as described in the main text. (b) Temperature dependence of $d(\Delta\chi_{\text{mag}})/dT$. (c) and (d) Doping dependence of γ' and reduced χ^2 for the fitting in (a). The vertical dashed line represents the crossover from first order to second order for the magnetic transition.

the broad peak can be fitted with two Lorentz functions with the same width, whose peak positions are labeled as T_N and T_s . It should be noted that these values show little change if one uses two Gaussian functions to fit the data. Figure 1(c) shows that T_N linearly depends on the nominal Ba doping x_{norm} , but deviation occurs even for samples with the same x_{norm} . This is most likely due to inhomogeneity during the crystal growth process. Therefore, we calculate the Ba doping level x in the following according to its T_N . The doping dependence of $T_s - T_N$ is shown in Fig. 1(d), which suggests that the separation between the two transitions becomes non-zero above $x = 0.41$ and then monotonically increases with increasing x .

Figure 2 gives the results of magnetic susceptibility χ_{mag} to determine the nature of the magnetic transition in $\text{Sr}_{1-x}\text{Ba}_x\text{Ni}_{0.03}\text{Fe}_{1.97}\text{As}_2$. The magnetic susceptibility for all samples studied here shows a linear temperature dependence above T_N ³³, which is subtracted from χ_{mag} to obtain $\Delta\chi_{\text{mag}}$. As shown in Fig. 2(a), while all the $-\Delta\chi_{\text{mag}}$ increase rapidly with decreasing temperature around T_N , the upturn looks sharper for lower doping (higher T_N) samples, suggesting a crossover from first to second order transition. This can be seen much clearer from $d(\Delta\chi_{\text{mag}})/dT$ as shown in Fig. 2(b), where the nature of the AF transition can be easily judged from both the height and width of the peak around T_N . Accordingly, the crossover from the first to second order transitions happens between $x = 0.41$ and 0.42 .

The nature of the magnetic transition can also be studied by fitting $-\Delta\chi_{\text{mag}}$ below T_N with a function of $\chi_0(1 - T/T_N)^{\gamma'}$. To account for the tail behavior above T_N , a Gaussian distribution of T_N has been included in the fitting³⁴. The Gaussian width σ is between 1K and 2 K for high doping samples, which is consistent

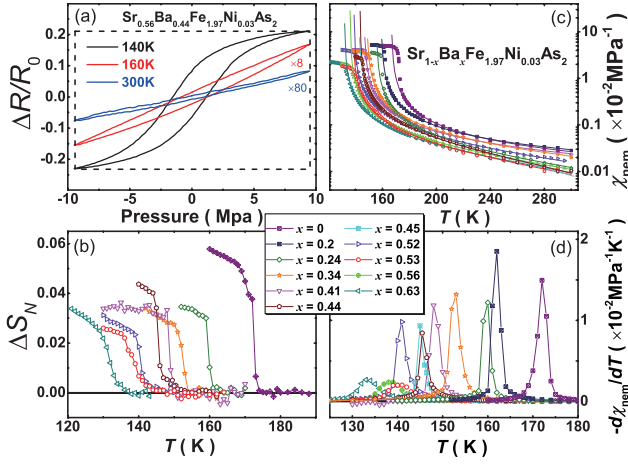


FIG. 3: (a) Resistivity change $\Delta R/R_0$ under uniaxial pressure along the (110) tetragonal direction for the $x = 0.44$ sample with $T_N = 145.8$ K. The dashed rectangular box indicates the total area used to normalized the hysteresis area at 140 K. (b) The temperature dependence of normalized area ΔS_N with constant high-temperature values subtracted. (c) Temperature dependence of nematic susceptibility χ_{nem} with log-scale vertical axis. The solid lines are fitted with the Curie-Weiss-like function as described in the main text. (d) Temperature dependence of $-d\chi_{\text{nem}}/dT$ that shows peak around the transition.

with previous studies by neutron diffraction for similar systems^{35,36}. The critical exponent γ' for most high doping samples is between 0.2 and 0.25. With decreasing Ba doping, γ' becomes much smaller for $x < 0.4$. More clearly, the reduced χ^2 measuring the goodness of fit increases sharply right below $x = 0.41$ as shown in Fig. 2(d), which accords with the expectation that the above function cannot fit a first order transition well.

After determining the nature of the magnetic transitions, we further investigate nematic transitions in these materials by studying nematic susceptibility χ_{nem} . Here, χ_{nem} is defined as $d(\Delta R/R_0)/dp$ as described previously³², where R_0 is the resistance at zero pressure and $\Delta R = R(p) - R_0$. It has been shown that χ_{nem} is directly associated with nematic transition in $\text{BaFe}_{2-x}\text{Ni}_x\text{As}_2$ ³². Figure 3(a) shows some of the raw data for the $x = 0.44$ sample. At 140 K that is smaller than T_N , a ferromagnetic-like hysteresis loop is observed most likely due to the presence of domains as in a ferromagnetic material. We define S_N as the area of the hysteresis loop divided by the minimum rectangular area that contains it as shown in the dashed box in Fig. 3(a). Figure 3(b) shows the temperature dependence of ΔS_N where the high-temperature constant values due to the intrinsic hysteresis of the piezo-bender has been subtracted³². A clear jump can be seen for lower-doping samples, suggesting a first order transition.

The temperature dependence of nematic susceptibility χ_{nem} is shown in Fig. 3(c). It should be noted that since χ_{nem} is not well defined below T_s due to the presence of a

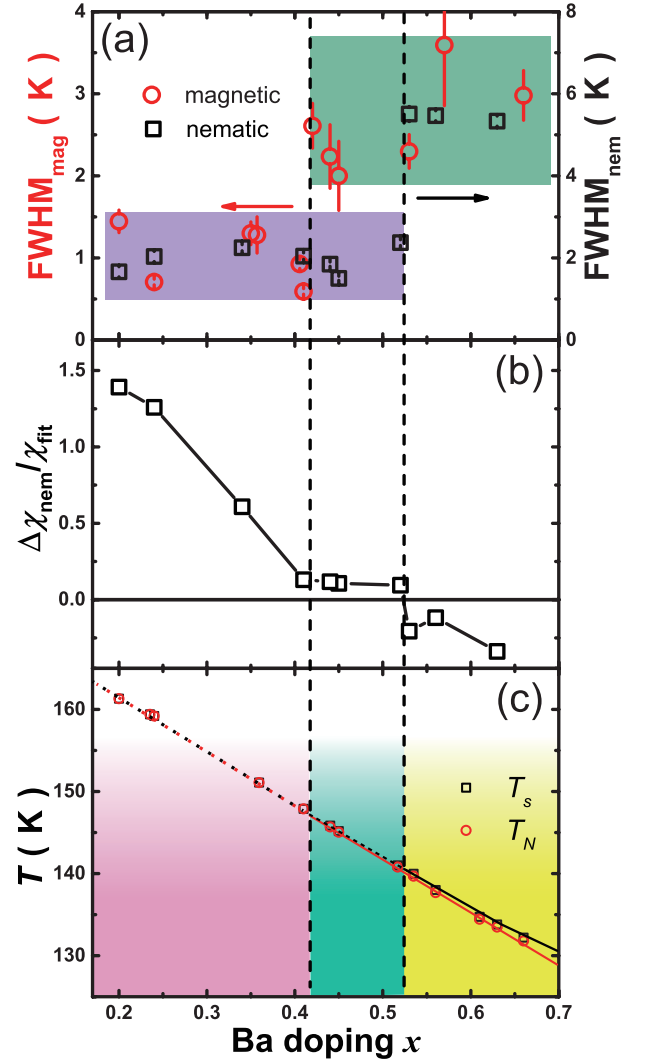


FIG. 4: (a) Doping dependence of FWHMs of the peaks in $d\Delta\chi_{\text{mag}}/dT$ (red circles) and $-d\chi_{\text{nem}}/dT$ (black squares) for the magnetic and nematic transitions, respectively. The vertical error bars are obtained from the fittings. (b) Doping dependence of nematic susceptibility jump $\Delta\chi_{\text{nem}}/\chi_{\text{fit}}$ at T_s . (c) Doping dependence of T_N (red circles) and T_s (black squares). The dotted and solid lines represent first order and second order transitions, respectively. The vertical dashed lines separate the phase diagram into three regions.

ferromagnetic-like hysteresis loop, we force a linear fit to the whole range of the data. Therefore, the data below T_s just represent a trend rather than the actual value of the nematic susceptibility. Similar to $d\chi_{\text{mag}}/dT$, the first derivative of χ_{nem} also shows a peak feature around T_s as shown in Fig. 3(d). The difference between sharp and broad peaks clearly suggests the difference between first order and second order transitions.

To quantitatively compare the nature of magnetic and nematic transitions, we show the doping dependence of FWHM of the peaks in Figs. 2(b) and 3(d) fitted by a Lorentz lineshape. With increasing Ba doping, the

FWHM associated with the magnetic transition jumps to about twice its value above $x = 0.41$, while a similar jump for the FWHM associated with the nematic transition happens above $x = 0.52$, as shown in Fig. 4(a). Accordingly, one can identify three regions. In region I ($x \leq 0.41$), both magnetic and nematic transitions are first order. In region III ($x \geq 0.53$), both of them are second order. In region II ($0.41 < x < 0.53$), the magnetic transition becomes second order while the nematic one remains first order, which has never been observed in other materials. Interestingly, FWHM_{nem} is always about twice as much as FWHM_{mag} in either region I or region III, which suggests a very close relationship between the AF and nematic orders.

For a first order nematic transition, one will expect a jump of nematic susceptibility around T_s . Such jump is obvious for lower doping samples with strongly first order nematic transition as shown in Fig. 3(c). The amplitude of the jump can be quantitatively analyzed by the value of $\Delta\chi_{\text{nem}}/\chi_{\text{fit}}$ at T_s , where χ_{fit} is the fitted value of a Curie-Weiss-like function as described previously³² and $\Delta\chi_{\text{nem}} = \chi_{\text{nem}} - \chi_{\text{fit}}$. Following the doping dependence of $\Delta\chi_{\text{nem}}/\chi_{\text{fit}}$ at the lower doping regime, it seems that its values will drop to zero at the crossover between region I and II as shown in Fig. 4(b). In region II, the jump becomes very small when the AF transition becomes second order even though the nematic transition itself is still first order.

Figure 4(c) gives the doping dependence of T_N and T_s . The separation between T_s and T_N [see Fig. 1(d)] coincides with the change of the AF transition from first to second order. The change of nematic order from first to second order [Fig. 4(a)] seems to have no effect on the size of the separation between T_N and T_s . The magnetic and nematic tricritical points can thus be identified at x of about 0.41 and 0.52, respectively. We note that neutron scattering experiments have reported a few of Kelvins enhancement of T_N and T_s under pressure^{30,36-38}, but it will not affect the position of the magnetic tricritical point and the separation of T_N and T_s since they were determined from measurements at zero pressure. Moreover, the pressure has a negligible effect in determining nematic tricritical point here since resistivity measurements under pressure show negligible change of T_N and T_s ³⁹ (see also Supplementary Materials⁴⁰). It is unclear why the results between resistivity and neutron scattering measurements are different, probably because the former use thin slices of crystals that are different from the large and almost square samples used in the latter.

The rich behaviors of the magnetic and nematic transitions in $\text{Sr}_{1-x}\text{Ba}_x\text{Ni}_{0.03}\text{Fe}_{1.97}\text{As}_2$ suggest that the intermediate phase with magnetic and nematic tricritical

points is crucial to distinguishing various theories²⁻¹⁴. To our knowledge, our results can only be explained by Ref.¹¹. While BaFe_2As_2 seems to be the case of moderate anisotropy^{6,28}, it has been pointed out that electron-doping results in more anisotropic spin correlations²⁵, suggesting that the phase diagram here is the same as that in Ref.¹¹ for the strong anisotropy case. Accordingly, the nature of the magnetic and nematic transitions are determined by the nematic coupling, which can be tuned by the change of either Fermi pockets^{41,42} or shear modulus^{43,44}. Moreover, it is predicted that the first order transition of nematic order cannot trigger a first order magnetic transition if the magnitude of the jump of its order parameter at T_s becomes too small, which is also consistent with the results in Fig. 4(b). The excellent consistency between our results and theoretical predictions demonstrates that the nematic order in this system is driven by the spin degree of freedom and suggests the importance of itinerant characteristics of electron system.

IV. CONCLUSIONS

In conclusion, an intermediate doping region has been unambiguously established in the $\text{Sr}_{1-x}\text{Ba}_x\text{Ni}_{0.03}\text{Fe}_{1.97}\text{As}_2$ system by studying the temperature dependence of resistivity and magnetic and nematic susceptibilities. In this region, although the nematic transition is still first order, the jump of the nematic order parameter becomes very small, which coincides with the crossover from first order to second order for the AF transition. Our results agree with the magnetic scenario for an itinerant fermionic model in excellent details.

V. ACKNOWLEDGMENTS

This work is supported by the Ministry of Science and Technology of China (No. 2017YFA0302903, No. 2016YFA0300502, No. 2017YFA0303103, No. 2015CB921302, No. 2015CB921303), the National Natural Science Foundation of China (No. 11674406, No. 11374346, No. 11774401, No. 11374011, No. 11674406, No. 11522435) and the Strategic Priority Research Program(B) of the Chinese Academy of Sciences (XDB07020300, XDB07020200, No. 11774401). H. L. and Y. Y. are supported by the Youth Innovation Promotion Association of CAS.

* Electronic address: slli@iphy.ac.cn

¹ R. M. Fernandes, A. V. Chubukov, and J. Schmalian, Nat.

Phys. **10**, 97 (2014).

² W. Lv, J. Wu, and P. Phillips, Phys. Rev. B **80**, 224506

- (2009).
- ³ C.-C. Lee, W.-G. Yin, and W. Ku, *Phys. Rev. Lett.* **103**, 267001 (2009).
 - ⁴ P. M. R. Brydon, M. Daghofer, and C. Timm, *J. Phys. Condens. Matter* **23**, 246001 (2011).
 - ⁵ W.-C. Lee, W. Lv, and H. Z. Arham, *Inter. J. Mod. Phys. B* **27**, 1330014 (2013).
 - ⁶ M. G. Kim, R. M. Fernandes, A. Kreyssig, J. W. Kim, A. Thaler, S. L. Budko, P. C. Canfield, R. J. McQueeney, J. Schmalian, and A. I. Goldman, *Phys. Rev. B* **83**, 134522 (2011).
 - ⁷ C. Fang, H. Yao, W.-F. Tsai, J. Hu, and S. A. Kivelson, *Phys. Rev. B* **77**, 224509 (2008).
 - ⁸ C. Xu, M. Mller, and S. Sachdev, *Phys. Rev. B* **78**, 020501 (2008).
 - ⁹ Y. Qi and C. Xu, *Phys. Rev. B* **80**, 094402 (2009).
 - ¹⁰ R. M. Fernandes, E. Abrahams, and J. Schmalian, *Phys. Rev. Lett.* **107**, 217002 (2011).
 - ¹¹ R. M. Fernandes, A. V. Chubukov, J. Knolle, I. Eremin, and J. Schmalian, *Phys. Rev. B* **85**, 024534 (2012).
 - ¹² A. L. Wysocki, K. D. Belashchenko, and V. P. Antropov, *Nat. Phys.* **7**, 485 (2011).
 - ¹³ Y. Kamiya, N. Kawashima, and C. D. Batista, *Phys. Rev. B* **84**, 214429 (2011).
 - ¹⁴ R. Applegate, R. R. P. Singh, C.-C. Chen, and T. P. Devereaux, *Phys. Rev. B* **85**, 054411 (2012).
 - ¹⁵ M. S. Torikachvili, S. L. Budko, N. Ni, and P. C. Caneld, *Phys. Rev. Lett.* **101**, 057006 (2008).
 - ¹⁶ N. Ni, S. Nandi, A. Kreyssig, A. I. Goldman, E. D. Mun, S. L. Budko, and P. C. Caneld, *Phys. Rev. B* **78**, 014523 (2008).
 - ¹⁷ E. Colombier, S. L. Budko, N. Ni, and P. C. Caneld, *Phys. Rev. B* **79**, 224518 (2009).
 - ¹⁸ M. Rotter, M. Tegel, D. Johrendt, I. Schellenberg, W. Hermes, and R. Pöttgen, *Phys. Rev. B* **78**, 020503(R) (2008).
 - ¹⁹ K. Kitagawa, N. Katayama, K. Ohgushi, M. Yoshida, and M. Takigawa, *J. Phys. Soc. Jpn.* **77**, 114709 (2008).
 - ²⁰ S. D. Wilson, Z. Yamani, C. R. Rotundu, B. Freelon, E. Bourret-Courchesne, and R. J. Birgeneau, *Phys. Rev. B* **79**, 184519 (2009).
 - ²¹ K. Matan, R. Morinaga, K. Iida, and T. J. Sato, *Phys. Rev. B* **79**, 054526 (2009).
 - ²² C. R. Rotundu, B. Freelon, T. R. Forrest, S. D. Wilson, P. N. Valdivia, G. Pinuellas, A. Kim, J.-W. Kim, Z. Islam, E. Bourret-Courchesne, et al., *Phys. Rev. B* **82**, 144525 (2010).
 - ²³ D. K. Pratt, W. Tian, A. Kreyssig, J. L. Zarestky, S. Nandi, N. Ni, S. L. Budko, P. C. Caneld, A. I. Goldman, and R. J. McQueeney, *Phys. Rev. Lett.* **103**, 087001 (2009).
 - ²⁴ S. Nandi, M. G. Kim, A. Kreyssig, R. M. Fernandes, D. K. Pratt, A. Thaler, N. Ni, S. L. Budko, P. C. Caneld, J. Schmalian, et al., *Phys. Rev. Lett.* **104**, 057006 (2010).
 - ²⁵ L. W. Harriger, A. Schneidewind, S. Li, J. Zhao, Z. Li, W. Lu, X. Dong, F. Zhou, Z. Zhao, J. Hu, et al., *Phys. Rev. Lett.* **103**, 087005 (2009).
 - ²⁶ H. Luo, R. Zhang, M. Laver, Z. Yamani, M. Wang, X. Lu, M. Wang, Y. Chen, S. Li, S. Chang, et al., *Phys. Rev. Lett.* **108**, 247002 (2012).
 - ²⁷ X. Lu, H. Gretarsson, R. Zhang, X. Liu, H. Luo, W. Tian, M. Laver, Z. Yamani, Y.-J. Kim, A. H. Nevidomskyy, et al., *Phys. Rev. Lett.* **110**, 257001 (2013).
 - ²⁸ C. R. Rotundu and R. J. Birgeneau, *Phys. Rev. B* **84**, 092501 (2011).
 - ²⁹ J. E. Mitchell, B. Sagarov, W. Lin, S. Calder, Q. Li, S. V. Kalinin, M. Pan, A. D. Christianson, and A. S. Sefat, *Phys. Rev. B* **86**, 174511 (2012).
 - ³⁰ X. Lu, K.-F. Tseng, T. Keller, W. Zhang, D. Hu, Y. Song, H. Man, J. T. Park, H. Luo, S. Li, et al., *Phys. Rev. B* **93**, 134519 (2016).
 - ³¹ Y. Chen, X. Lu, M. Wang, H. Luo, and S. Li, *Supercond. Sci. Technol.* **24**, 065004 (2011).
 - ³² Z. Liu, Y. Gu, W. Zhang, D. Gong, W. Zhang, T. Xie, X. Lu, X. Ma, X. Zhang, R. Zhang, et al., *Phys. Rev. Lett.* **117**, 157002 (2016).
 - ³³ X. F. Wang, T. Wu, G. Wu, H. Chen, Y. L. Xie, J. J. Ying, Y. J. Yan, R. H. Liu, and X. H. Chen, *Phys. Rev. Lett.* **102**, 117005 (2009).
 - ³⁴ R. Birgeneau, H. Guggenheim, and G. Shirane, *Phys. Rev. B* **8**, 304 (1973).
 - ³⁵ W. Zhang, J. T. Park, X. Lu, Y. Wei, X. Ma, L. Hao, P. Dai, Z. Y. Meng, Y. feng Yang, H. Luo, et al., *Phys. Rev. Lett.* **117**, 227003 (2016).
 - ³⁶ C. Dhital, T. Hogan, Z. Yamani, R. J. Birgeneau, W. Tian, M. Matsuda, A. S. Sefat, Z. Wang, and S. D. Wilson, *Phys. Rev. B* **89**, 214404 (2014).
 - ³⁷ C. Dhital, Z. Yamani, W. Tian, J. Zeretsky, A. S. Sefat, Z. Wang, R. J. Birgeneau, and S. D. Wilson, *Phys. Rev. Lett.* **108**, 087001 (2012).
 - ³⁸ Y. Song, S. V. Carr, X. Lu, C. Zhang, Z. C. Sims, N. F. Luttrell, S. Chi, Y. Zhao, J. W. Lynn, and P. Dai, *Phys. Rev. B* **87**, 184511 (2013).
 - ³⁹ I. R. Fisher, L. Degiorgi, and Z. X. Shen, *Rep. Prog. Phys.* **74**, 124506 (2011).
 - ⁴⁰ See Supplemental Material at <http://link.aps.org/supplemental/10.1103/PhysRevB.96.104514> for discussions on the change of T_N and T_s under pressure, and error bars in Fig. 4(a).
 - ⁴¹ Y. Zhang, J. Wei, H. W. Ou, J. F. Zhao, B. Zhou, F. Chen, M. Xu, C. He, G. Wu, H. Chen, et al., *Phys. Rev. Lett.* **102**, 127003 (2009).
 - ⁴² L. X. Yang, Y. Zhang, H. W. Ou, J. F. Zhao, D. W. Shen, B. Zhou, J. Wei, F. Chen, M. Xu, C. He, et al., *Phys. Rev. Lett.* **102**, 107002 (2009).
 - ⁴³ W. O. Uhoya, J. M. Montgomery, G. M. Tsoi, Y. K. Vohra, M. A. McGuire, A. S. Sefat, B. C. Sales, and S. Weir, *J. Phys. Condens. Matter* **23**, 122201 (2011).
 - ⁴⁴ J. E. Jorgensen and T. C. Hansen, *Eur. Phys. J. B* **78**, 411 (2010).